

Action at a Distance: A Key to Homopolar Induction

R. Achilles & J. Guala-Valverde

Applied Physics Group, Confluencia Tech University
Fundación J. Palacios Neuquén Q8300JFL, Argentina
e-mail: <achilles@ieee.org> web-p: www.fjp.org.ar

The crucial character of relative motion and Ampère's force law in interpreting homopolar induction was pointed out in recent experimentation performed by us. H. Montgomery suggests the compatibility of that experimental results with Maxwell's field theory. With the purpose of elucidating the applicable rationale this article identifies three independent energy-conversion mechanisms definable within the basic homopolar-machine frame and, hinging on a specially developed finite-element software, introduces an Ampèrian analysis of associated electro- and ponderomotive effects.

Keywords: Homopolar Induction – Field Theory – Action at a Distance – Relativity – Action and Reaction

1. Introduction

At the 19th Century, Faraday's experimentation on electromagnetic induction opened the era of electromechanical energy conversion [1]. At that time, however, the requirement of having relative motion between a machine's constitutive parts (cylinder-piston, stator-rotor,

magnet-disk, etc.) to convert energy to or from mechanical into other forms was not as obvious as nowadays [2].

Faraday himself interpreted his experiments in terms of magnetic field “force lines” before the mathematical formulation of the field theory by Maxwell [3]. This theory, complemented by further developments of Hertz, Heaviside and Lorentz, used the concept of magnetic field –a physical attribute assigned to the space surrounding magnetic sources- to explain nearly all electromagnetic phenomena. The Newtonian remote-action Ampère’s force law describing the mechanical interaction between elementary current paths [4] became in such scenario disregarded.

The alternative unsymmetrical force law proposed in 1845 by Grassmann [5] –satisfying the new field theory but violating Newton’s third law- was used almost to the exclusion of all others during the last century. Its further generalization to include free charges in motion enabled define the magnetic force component of the modern Lorentz force expression [6].

In our opinion, the outcoming dominant unsymmetrical treatment of electrical machines since, and the still open controversy on the applicable force law stand as salient facts still darkening present-days interpretation of homopolar induction physics.

As it happened with Grassmann’s law, the initial lack of generality of Ampère’s law was complemented by contributions of others as Neumann and Weber [7,8,9,10]. Today’s massive availability of computer analysis means in concomitance with better experimental facilities allow update the interpretation of the phenomenon’s relevant physics as defined by the two theories in conflict. Such a study is carried out in this article.

2. Grassmann versus Ampère

Ampère's force law draws an expression for the magnitude of the mechanical forces mutually applied between two current elements $i_m d\vec{m}$ and $i_n d\vec{n}$ separated a distance \vec{r}_{mn} [11]. Calling ε the intra-element angle, and α and β the angles between each element and the distance vector, its magnitude for the coplanar case depicted in Figure 1 is described by:

$$d^2 F_{mn} = -\frac{\mu_0 i_m i_n}{4\pi \cdot r_{mn}^2} (2 \cos \varepsilon - 3 \cos \alpha \cdot \cos \beta) dm \cdot dn \quad (1)$$

The $d^2 F_{mn}$ force obeys Newton's third law being its direction coincidental with the one of the distance vector. Attraction occurs for a negative $d^2 F_{mn}$ magnitude.

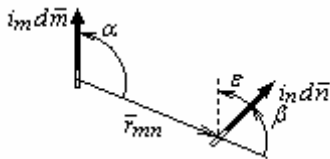


Figure 1 – Coplanar Current Elements

For the same arrangement, the Grassmann's law vector expressions for the forces acting on each element are:

$$d^2 \vec{F}_m = \frac{\mu_0 i_m i_n}{4\pi \cdot r_{mn}^3} d\vec{m} \times (d\vec{n} \times \vec{r}_{mn}) \quad (2)$$

$$d^2 \vec{F}_n = \frac{\mu_0 i_m i_n}{4\pi \cdot r_{mn}^3} d\vec{n} \times (d\vec{m} \times \vec{r}_{mn}) \quad (3)$$

In line with Biot-Savart's law, the vector products between brackets define the normal to the plane direction of the magnetic field

created by each element in the position of the other. The typically unmatched direction of the coplanar forces $d^2\bar{F}_m$ and $d^2\bar{F}_n$ defined by –respectively– the vector product of the $i_m d\bar{m}$ element by the $i_n d\bar{n}$ magnetic field and vice versa, gives rise to a mechanical torque applied to the system.

But, the more striking differences between both viewpoints can be grasped from an array consisting of a current element $i_n d\bar{n}$ that held parallel to itself and to another element $i_m d\bar{m}$ at rest, describes a circle around it. The first-quadrant $d^2\bar{F}_{nm}$ forces on the turning element for both theories were plotted in Figure 2 at intervals of 10° of the element-distance angle α . A force of the same magnitude and opposite direction acts in each case on the element at rest.

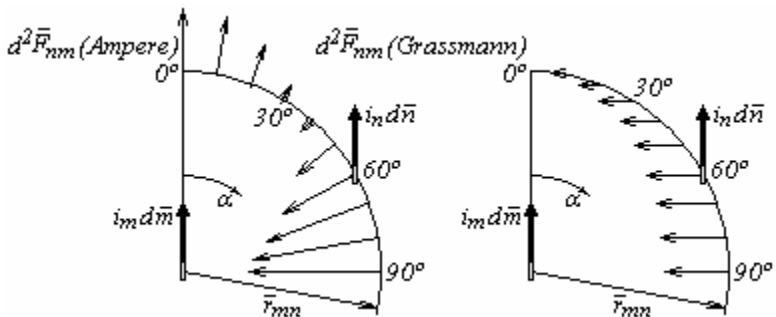


Figure 2 – Ampère's and Grassmann's Force Polar Diagrams

The no-Newtonian character of the Grassmann's elementary forces is depicted by its invariant horizontal direction. However, it has been demonstrated that its integration along closed trajectories cancels the observed unaligned force components, being in such case Newton's third law verified [12].

With $\varepsilon = 0$ in all cases and α defining the angle between each element and the distance vector \bar{r}_{mn} , as compared to Grassmann's Ampère forces may be defined as:

- attractive, duplicated in magnitude for $\alpha = 90^\circ$,
- nullified for $\alpha = \cos^{-1}[(2/3)^{1/2}] = 35.3^\circ$,
- repulsive with half of the $\alpha = 90^\circ$ magnitude, in contrast to the zeroed Grassmann forces for $\alpha = 0^\circ$.

Beyond the closed-circuit compliance of Newton's third law by both approaches, the pointed out differences in force direction and magnitude at current-element level fire up existing homopolar-induction controversies. A not minor point here is the existence of longitudinal forces, confirmed in the past by the Ampère's bridge and in modern times the object of measurements of conductor-wire traction and breakage, electrical-gun rail buckling, etc. by Graneau and others [11,13,14].

3. The Homopolar Machine

The impact of both theories on homopolar induction may be evaluated on the original machine frame, namely a conductive disk attached to the end of a shaft aligned and having relative motion with respect to a cylindrical magnet creating an axial magnetic field \bar{B} . A third part, the external conductor –closing a circuit by simultaneous contact with a radially inner and an outer position of the disk, enables the measurement of generated electromotive forces or the injection of ponderomotive currents from an external source into the disk.

Materially, assuming relative motion among all three described parts, two subsidiary homopolar machines are identified: the magnet-disk machine **H1** and the magnet-conductor machine **H2**. The first, of utmost mutual inductance, exhibits the higher energy-conversion rate. A third electrodynamic machine (**E1**) of much lesser power, enabled

to operate only as a motor, is defined for the disk-conductor combination.

The mutual anchoring of any two machine constitutive parts disables the respective energy-conversion mechanism, with the remaining subsets taking the torque- and electromotive-force production actions.

A centripetal current i_m injected in the disk by an external circuit anchored to the magnet gives place to the **H1** machine operation in motor mode (M-mode) where, according to Grassmann, a tangential force $\bar{F}_m = \int_0^R i_m d\bar{m} \times \bar{B}$ rotates the disk converting electrical into mechanical energy (see Figure 3).

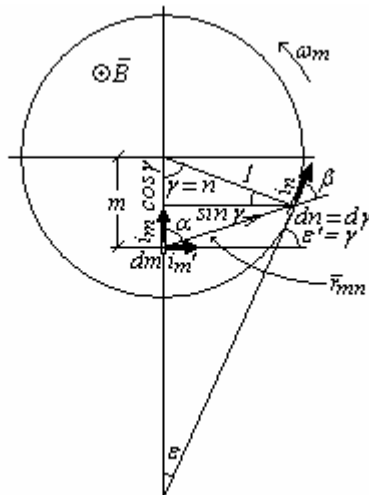


Figure 3 – Current-Element Geometry

Alternatively, the rotation by an external mechanical power source of the disk and its free charges (current i_m') relative to the magnetic field, applies radial Grassmann-Lorentz forces on the moving charges. The disk radial electromotive force associated to the

displaced-charge electrical field, $\varepsilon = \int_0^R (\bar{v} \times \bar{B}) \cdot d\bar{m} = \omega_m B \int_0^R m \cdot dm$, sets up the operation of **H1** in generator mode (G-mode). The connection through the external conductor of any two radially distant points of the disk, enables the conversion of mechanical energy into electrical.

The system was formulated based on the \bar{B} -equivalent spin-orientation ring current i_n , the injected centripetal current i_m for M-mode, and the tangential charge-displacement current i_m' for G-mode. The proportionality $Force \equiv Current^2$ detected by Ampère [10] allows to consider a magnet and disk unitary radius. While 360 elements of $\pi/180$ length were taken for the circumferential current trajectories of i_n and i_m' , the unitary radius was divided in 80 incrementals for finite-element calculations associated to the radial current i_m . The separation distance between a radial element located at m and a circumferential element positioned in γ (or n), verifies:

$$r_{mn}^2 = m^2 + 1 - 2m \cdot \cos \gamma \quad (4)$$

where the interacting Ampèrian forces for M- and G-mode are:

$$\Delta^2 F_{mn} (M) = -\frac{\mu_0 i_m i_n}{4\pi \cdot r^2} (2 \cos \varepsilon - 3 \cos \alpha \cos \beta) \Delta m \cdot \Delta n \quad (5)$$

with:

$$\cos \varepsilon = \sin \gamma, \quad \cos \alpha = (m - \cos \gamma) r_{mn}^{-1} \quad \text{and} \quad \cos \beta = m \cdot \sin \gamma \cdot r_{mn}^{-1} \quad (6)$$

and:

$$\Delta^2 F_{mn} (G) = -\frac{\mu_0 i_m' i_n}{4\pi \cdot r^2} (2 \cos \varepsilon' - 3 \cos \alpha' \cos \beta) m \cdot \Delta n^2 \quad (7)$$

with:

$$\cos \varepsilon' = \cos \gamma \quad \text{and} \quad \cos \alpha' = \sin \alpha = \sin \gamma \cdot r_{mn}^{-1} \quad (8)$$

While the magnet's spin-orientation equivalent current i_n was calculated from the expression of the magnetic field at the center of a current-carrying loop $B = \mu_0 i_n (2R)^{-1}$, the charge-displacement current i_m' was estimated based on the movement at rotational speed ω_m of half of highest-possible disk charge density ρ permitted by the air's dielectric strength $3.0E6 \text{ NC}^{-1}$. Consequently, the displacement current magnitude of a disk element of thickness t located at a radial position m turning at speed ω_m is calculated for the electrical charge q_m' stored in the elementary volume $t \cdot m \Delta m \Delta n$ as:

$$i_m' = \frac{q_m' m \omega_m}{m \Delta n} = \frac{\rho}{2} t \cdot \omega_m m \Delta m \quad (9)$$

The here developed homopolar-machine steady-state analysis is coplanar. By one side it is an acceptable criteria for confined-field machines of higher interest to the industry, and by the other it configures a simpler analysis of the same physics governed –in the case of disk and magnet circuits located at different axial positions– by the respective radial and tangential Ampère force component ruling electro- and ponderomotive effects.

Besides, in the coplanar case the computation of equations (5) and (7) draws undefined elementary force magnitudes at the $m=1, n=0$ singular point where the intra-element distance r_{mn} , and the Δm and Δn magnitudes tend simultaneously to zero. While it was solved by Wesley with current-density considerations [10], we opted for calculating the $\Delta^2 F_{mn}$ limit value at the $m=1, n=0^+$ side of the point assuming both elements approaching zero at the same speed (i.e. $\Delta m = \Delta n$ with $r_{mn}^2 = 0.5 \Delta m^2$), with a similar consideration made for the $m=1, n=0^-$ side.

$$\Delta^2 T_m (M) = \Delta^2 F_{mn} (M) \sin \alpha \cdot mR \quad (13)$$

$$\Delta^2 T_n (G \& M) = \Delta^2 F_{mn} (G \& M) \cos \beta \cdot R \quad (14)$$

where the equality $m \sin \alpha = m \cos \alpha' = \cos \beta$ derived from equations (6) and (8) confirms Newton's third law compliance by elementary and global machine torques for both operating modes.

And, in line with Neumann's elemental law of induction [11] net radial electromotive forces on the disk, and tangential electromotive forces on the magnet, are obtained from the integration of:

$$\Delta^2 \mathcal{E}_m (G) = \frac{m\omega_m R}{i_m'} \Delta^2 F_{mn} (G) \sin \alpha' \quad (15)$$

$$\Delta^2 \mathcal{E}_m (M) = \frac{m\omega_m R}{i_m} \Delta^2 F_{mn} (M) \cos \alpha \quad (16)$$

$$\Delta^2 \mathcal{E}_n (G \& M) = -\frac{\omega_m R}{i_n} \Delta^2 F_{mn} (G \& M) \cos \beta \quad (17)$$

The described finite-element methodology was implemented in the form of a Fortran executable image, the Program H-Mac. It is oriented to the calculation of mechanical and electromotive forces and torques applied to the machine constitutive parts in open-circuit G-mode and in blocked-rotor (i.e. disk attached to the magnet) M-mode operation. It is complemented by a graphic environment exhibiting the distribution of disk and magnet incremental forces for both operating modes.

After the data-input session, the alphanumeric output prompts a comparative table of net mechanical-force, electromotive-force and torque magnitudes applied to a radial path of the disk and to the magnet's periphery for both theories.

4. Discussion of Results

An example, consisting of a 1.0 T magnet with a 20 cm-radius copper disk of 2 mm thickness turning counterclockwise at 50 r/s for generator operation, and injected with a 10 A centripetal current for motor operation, was applied as testing case.

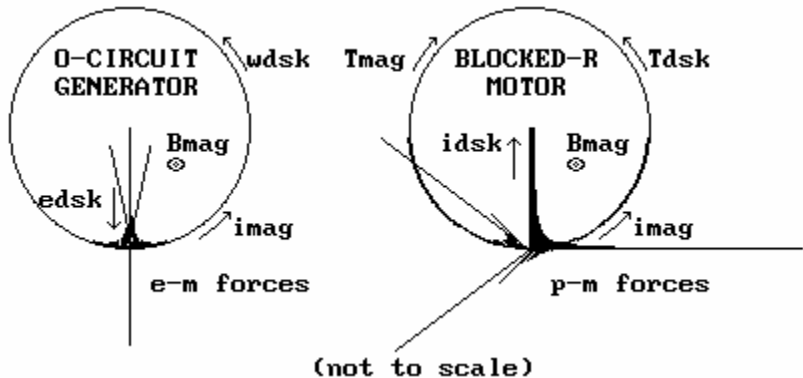


Figure 5 – Ampère's Incremental Forces on Disk and Magnet

The program's graphic output exhibited in Figure 5 depicts the Ampèrian elementary electro- and ponderomotive forces distribution on a disk radial path and on the magnet periphery for both operating modes analyzed. Each elementary force represented is the resultant of that element's interaction with all elements of its inductive counterpart (i.e. the magnet's 360 peripheral elements and the disk's 80 radial elements). The open-circuit generator and blocked-rotor motor conditions considered were selected in line with usual conventional-machine testing routines. It is interesting to observe the absence of tangential forces in the open-circuit generator (that would appear if the external circuit is closed) and the elimination of radial forces for the blocked-rotor motor (that would appear producing counter-electromotive forces if the disk is released from the magnet).

Besides, the introduced diagram becomes instrumental to visualize –for machine-design purposes- where major inductive effects are located. Clearly, that region can be identified as the one surrounding the singularity.

	Ampere		Grassmann	
	G-Mode *	M-Mode **	G-Mode *	M-Mode **
Fmag(radial)	0.155E-6 N	0 N	-	-
Fdisk(radial)	-0.155E-6 N	0 N	-0.927E-09 N	0 N
Fmag(tang)	0 N	-6.884 N	-	-
Fdisk(tang)	0 N	6.884 N	0 N	2.000 N
emag(ccw)	0 V	0 V	-	-
edisk(centrif)	3.166 V	0 V	1.000 V	0 V
Tmag(ccw)	0 Nm	-0.741 Nm	-	-
Tdisk(ccw)	0 Nm	0.741 Nm	0 Nm	0.200 Nm

* Open-Circuit Disk

** Mechanically Blocked Rotor

The table above exhibits the program's alphanumeric output. The calculated Ampèrian generator radial forces and motor tangential forces and torques applied on disk and magnet verify Newton's third law. The closure of an external circuit in the generator case would introduce –via the circulating disk current- equilibrated tangential forces on disk and magnet and a magnet's magnetizing peripheral electromotive force. Similarly, the motor's rotor release would introduce –via the enabled disk-magnet relative rotation- equilibrated radial forces, a disk counter-electromotive force and a magnet's demagnetizing electromotive force. Both, G-mode magnetizing and M-mode demagnetizing electromotive forces –trying to keep machine voltage and machine speed constant- verify besides the Faraday-Lenz law [1]. Conversely, for the Grassmann's approach there are neither mechanical forces nor torques or electromotive forces on the magnet for none of the operating modes analyzed. The aforementioned precludes the compliance of Newton's third law, energy conservation and Faraday-Lenz law by this latter theory.

Figure 5 confirms the incremental-force peak magnitudes in the $m=1$, $\gamma=0$ singularity encouraging the application of larger disk than magnet radii to increase radically machine power by utilizing the disk

$m=1^+$ radial region. Besides, the steep decrease of force magnitude far off the singularity in both disk-radial and magnet-peripheral senses, favours the adoption of annular-shaped disks with multiple radial circuits to attain –via the multiplication of singularities- a high-power homopolar machine.

5. A Homopolar-Induction Concept Map

Two decades ago, the interaction of new information with pre-existing knowledge was typified by Ausubel as significant learning [15]. A practical approach to implement such interaction, the concept map, was introduced later by Novak [16]. The homopolar-machine underlying physics identified experimentally and quantified in the here introduced steady-state analysis are condensed in the self-explanatory Novak concept map shown in Figure 6.

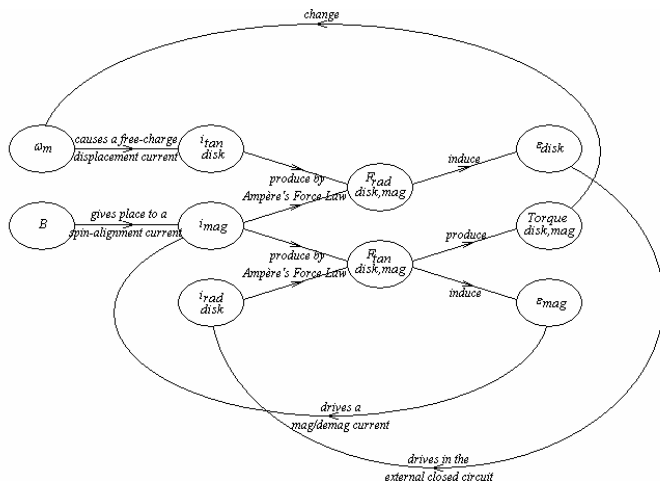


Figure 6 – Homopolar-Machine Operation Concept Map

Here, ω_m represents the disk rotational speed relative to the magnet. The $F_{tan}-\epsilon_{mag}-i_{mag}$ loop is excluded for Grassmann's

formulation, remaining the associated “constant” \overline{B} field outside the possibility of verifying Newton’s third law, energy conservation and Faraday-Lenz as it happens for the action-at-a-distance case.

A homopolar-machine dynamic model, including electrical-load resistance and inductance for G-mode, and mechanical-load inertia and friction for M-mode, will allow extend the present analysis to the transient state drawing additional grounds of the device’s subliminal physics.

References

- [1] M. Faraday, *Experimental researches in electricity*, B. Quaritsch, London. (1839).
- [2] R. Achilles, “Again on the Guala-Valverde homopolar induction experiments”, *Spacetime & Substance* **3** (2002) 235.
- [3] J. Maxwell, *A treatise on electricity and magnetism*, Clarendon Press, London (1891).
- [4] A. Ampère, “La détermination de la formule qui représente l’action mutuelle de deux portions infiniment petites de conducteur voltaïques”, *L’Académie Royale des Sciences* (1822).
- [5] H. Grassmann, “A new theory of electrodynamics”, *Poggendorf’s Annalen* **64** (1845) 1.
- [6] H. Lorentz, *The theory of electrons*, Teubner, Leipzig (1909).
- [7] F. Neumann, “Ueber ein allgemeines Prinzip der mathematische Theorie inducierter elektrischer Stroeme”, *Akademie der Wissenschaften*, Berlin (1847).
- [8] W. Weber, *Elektrodynamische Maasbestimmungen ueber ein allgemeines Grundgesetz der elektrische Wirkung*, Wilhelm Weber’s Werke, Springer, Berlin (1893).
- [9] P. Graneau, *Ampère-Neumann electrodynamics of metals*, Hadronic Press, Palm Harbor, FL (1994).
- [10] A. Assis, *Weber’s electrodynamics*, Kluwer, Dordrecht (1994).
- [11] P. Graneau, N. Graneau, *Newtonian electrodynamics*, World Scientific, Singapore (1996).

- [12] E. Whittaker, *A history of the theories of ether and electricity*, Thomas Nelson, London (1951).
- [13] A. Assis, “On the mechanism of railguns”, *Galilean Electrodynamics* **3** (1992) 93.
- [14] R. Achilles, “Field theory fictions and ghosts”, *Spacetime & Substance* **4** (2004) 162.
- [15] D. Ausubel, *Educational psychology: a cognitive view*, Holt, Rinehart & Wilson, New York (1988).
- [16] J. Novak, A. Cañas, “The theory underlying concept maps and how to construct them”, *Florida Institute for Human and Machine Cognition* **1** (2006).